ACS Catalysis

Research Article

pubs.acs.org/acscatalysis

QM/MM Calculations Revealing the Resting and Catalytic States in Zinc-Dependent Medium-Chain Dehydrogenases/Reductases

Gaurao V. Dhoke, Mehdi D. Davari, Ulrich Schwaneberg, and Marco Bocola*

RWTH Aachen University, Chair of Biotechnology, Worringer Weg 3, D-52074 Aachen, Germany

Supporting Information

ABSTRACT: Oxido-reductases from medium-chain dehydrogenase/reductase (MDR) family are excellent biocatalysts for the generation of optically pure alcohols from prochiral ketones. The mechanism of hydride and proton transfer steps in zinc-catalyzed carbonyl reduction has been investigated by quantum mechanical/molecular mechanical (QM/MM) calculations. The recent X-ray structure of zinc-dependent carbonyl reductase from *Candida parapsilosis* (CPCR2; PDB ID 4C4O) shows two different conformers of Glu66 and two positions of the catalytic zinc ion. Starting from four different hypothetical states, we obtained only two minima, so-called Zn_{rest}−Glu_{in} and Zn_{cat}−Glu_{out} of zinc ion and Glu66, indicating a coupled movement. We analyzed the dependence of barriers for the hydride transfer for these two states in the reduction of carbonyl substrate using QM/MM steered molecular dynamics (SMD) simulations. Our calculations show that the catalytic state (Zn_{cat}−Glu_{out}) has a ∼20 kcal/mol lower reaction barrier in comparison to the resting state (Zn_{rest}−Glu_{in}). This indicates that the coupled movement of zinc ion and Glu influences not only the ligand exchange but also the catalytic process of MDRs.

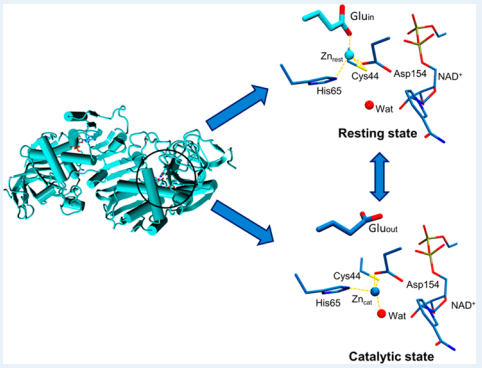

KEYWORDS: *QM/MM simulation, hydride transfer, steered molecular dynamics (SMD) simulation, ADH (alcohol dehydrogenase), MDR (medium chain dehydrogenase/reductase), carbonyl reduction*

1. INTRODUCTION

Alcohol dehydrogenases (ADHs) catalyze the reversible oxidation of primary and secondary alcohols to corresponding carbonyl compounds such as aldehydes or ketones[1−3] using $NAD(P)^+$ as a cofactor. In particular, the medium-chain dehydrogenase/reductase (MDR) family contains valuable oxido-reductases that have been proven to be excellent for the biocatalytic generation of optically pure alcohols from prochiral ketones.[4−6] Alcohol dehydrogenase from *Candida parapsilosis* (CPCR2; EC 1.1.1.1) was described to be a suitable catalyst for the asymmetric reduction of carbonyl substrates such as aliphatic and aromatic ketones, diketones, and keto acids.[7−9] The recently solved homotetrameric structure of ADH from *Candida parapsilosis* (CPCR2)[10] consists of two subunits (each 36 kDa) and belongs to the zinc-containing MDR family of ADHs. The MDR family of ADHs contains two zinc ions: one zinc ion is involved in catalysis, so-called catalytic zinc, while the other maintains the structural integrity of the enzyme, so-called structural zinc.[11] The oxidation mechanism of alcoholic substrate by zinc-dependent ADHs involves two steps: initially a chain of sequential events of proton transfers (PTs) followed by a hydride transfer (HT) step from the alcoholic substrate to the NAD^+ cofactor.[12,13]

In MDRs, catalytic zinc ion coordination varies in different combination of Cys, His, and Cys/Asp residues, but most commonly occurring is Cys-His-Cys, which forms the first shell of the catalytic zinc ion. The residues in the first shell of catalytic zinc maintain the stability of the metal complex and determine the selectivity along with the ligand binding mode.[14,15] However, the residues in the second shell of the catalytic zinc ion play an important role in protein−metal recognition and contribute energetically to the stabilization of the metal complex.[16−18] A recent study by Tiwari et al.[19] shows that conserved second shell Gly77 residue maintains the electronic and geometrical flexibility at the first coordination shell of the zinc ion during catalysis, highlighting the role of second-shell residues in MDRs. Glutamic acid (Glu) residue present in the second shell of the catalytic zinc is one of the conserved residues in the family of ADHs.[20,21] It is located on the side opposite to the substrate binding pocket behind the catalytic zinc. In horse liver alcohol dehydrogenase (HLADH), Glu68 is located at a distance of 4.70 Å behind the catalytic zinc. It has been already reported that Glu68 in HLADH plays an important role in enzyme catalysis and facilitates the exchange of ligands by coordination to the zinc ion when the old ligand dissociates.[22] Mutation of Glu68 to glutamine in HLADH[22,23] decreases the activity 100 times in comparison to wild type. A similar decrease in enzyme activity has been reported by mutation of conserved Glu60 residue to alanine (E60A-TbADH) and aspartate (E60D-TbADH) in ADH from

Received: October 6, 2014
Revised: April 17, 2015
Published: April 17, 2015

DOI: 10.1021/cs501524k
ACS Catal. 2015, 5, 3207−3215

Thermoanaerobacter brockii (TbADH).[24] A study on human glutathione dependent formaldehyde dehydrogenase (FDH) clarifies the role of the conserved Glu residue in a ligand exchange mechanism.[25] The furfural reduction in a zinc-dependent ADH from *Cupriavidus necator*[26] involves the rotational movement of two domains. The crystal structure of the closed form shows no coordination between Glu66 and catalytic zinc ion, while in the apo (open) form, Glu66 remains coordinated to catalytic zinc ion. This was proposed to facilitate the release of product and exchange of cofactor and explains the reduction in the overall enzymatic activity upon mutation of conserved glutamate residue in MDRs.[24,27] Structural studies on human glutathione dependent formaldehyde dehydrogenase (FDH) revealed that the catalytic zinc ion is located in two positions.[28] It has been postulated that movement of the catalytic zinc ion assists ligand substitution at the active site during the catalytic cycle[22] in HLADH. In addition for other zinc-dependent dehydrogenases, evidence for zinc ion movement were observed.[29,30] In ADH from *Sulfobolus solfataricus*,[30] catalytic zinc is directly coordinated to the Glu69 in the apoenzyme, while in the holoenzyme, the side chain of Glu69 is located 5.1 Å away from the catalytic zinc. In the X-ray structure of CPCR2[10] (PDB ID 4C4O), two different conformers for the conserved residue Glu66 (Glu_{in} and Glu_{out}) and two different positions of catalytic zinc ion (Zn_{rest} and Zn_{cat}) are observed (see Figure 1).

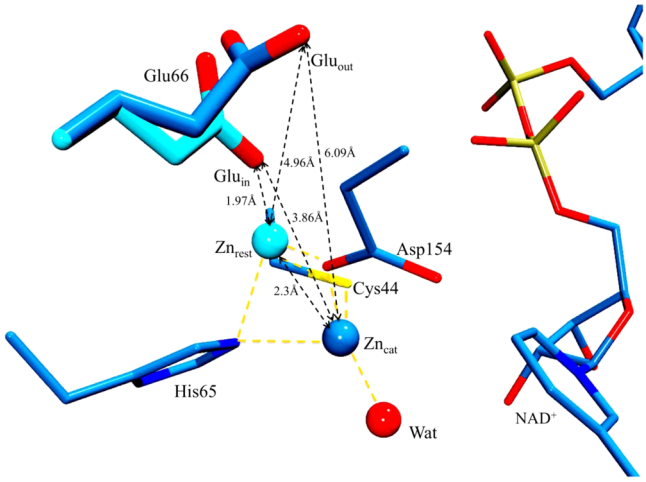

Figure 1. Catalytically active site of X-ray structure of CPCR2 (PDB ID 4C4O). All of the coordinating residues (Cys44, His65, and Asp154) with coordination bond (yellow) and the crystal water as fourth ligands are seen. Two positions of catalytic zinc (Zn_{cat} and Zn_{rest}) and two different conformers of Glu66 (Glu_{in} and Glu_{out}) are observed.

In this study, we investigate the role of the two conformers of Glu66 and two catalytic zinc ion positions found in the crystal structure of CPCR2, using a quantum mechanical/molecular mechanical (QM/MM) approach.[31] First, we performed the geometry optimization of the active site for two different conformers of Glu66 and two different positions of catalytic zinc ions to identify the corresponding minima. We then carried out QM/MM steered molecular dynamics (SMD) simulations to quantify the effect of different conformers of Glu66 on the barriers to hydride transfer from NADH cofactor to the carbonyl substrate. Our calculations identified two minimum energy states, the so-called resting state (Zn_{rest}–Glu_{in}) and catalytic state (Zn_{cat}–Glu_{out}), and the catalytic state has a lower barrier (20 kcal/mol) in comparison to the resting state for the hydride transfer step.

2. COMPUTATIONAL DETAILS

2.1. System Preparation. The initial starting structure was obtained from the X-ray crystal structure of CPCR2 (PDB ID 4C4O).[10] CPCR2 forms a tetrameric quaternary structure, consisting of two close dimers; therefore, a dimeric structure of CPCR2 was used as a starting point for all calculations. The protonation states of all residues apart from the zinc-coordinating residues (Cys44, His65, and Asp154) were determined using H^{++} protonation state calculation server.[32] All Glu and Asp residues were defined as being negatively charged, while Lys and Arg were positively charged. The protonation states of histidine residues for HID/HIE values were assigned on the basis of a hydrogen bonding network; His49 and His161 have protons on both nitrogens, His65, His45, and His161 have a proton on the Nδ position, and all other His residues have a proton on the Nε position. The cysteine residues coordinated to the structural zinc ion, Cys95, Cys98, Cys101, and Cys109, were treated as being negatively charged, while other cysteine residues were treated as being neutral. We used the SLEF approach, which is a nonbonded approach, to treat zinc interactions.[33] The input files were generated using the antechamber module in combination with the general amber force field (GAFF).[34] The amber force field parameters (force constants for bonds and angles) for nicotinamide cofactor NAD^+ were taken from the literature.[35,36] The hydrogen atoms were added by using the tleap module in Amber12,[37] and the Amber99SB force field[38,39] for the protein was employed. The protein was surrounded by a 12 Å rectangular box of TIP3P water molecules.[40] The system was then neutralized by adding 6 Na^+ ions. The complete CPCR2 simulation setup contains 66638 water molecules and 210145 atoms overall.

2.2. QM/MM Geometry Optimizations. On the basis of the atomic coordinates obtained from the X-ray structure of CPCR2 (PDB ID 4C4O), showing two different positions for zinc ion (Zn_{rest} and Zn_{cat}) and two different conformers of the residue Glu66 (Glu_{in} and Glu_{out}), four different model systems (Zn_{rest}–Glu_{in}, Zn_{rest}–Glu_{out}, Zn_{cat}–Glu_{in}, Zn_{cat}–Glu_{out}) were constructed as starting states for QM/MM calculations. The QM region (shown in Figure 2) consists of the side chains of zinc-coordinating residues (Cys44, His65, and Asp154) along with water as a fourth ligand, a part of the cofactor (NAD^+), Ser46 and His49, Glu66, and Arg331. The amino acid residues were cut between Cα and Cβ carbon. The NAD^+ cofactor was cut after the ribose moiety, as it is involved in the catalytic hydrogen bond network toward His49. Electrostatic embedding with a cutoff of 8 Å was used to maintain the interactions between QM and MM regions, and the link atom method[41] was used to maintain the valency of QM boundary atoms. All protein residues and the crystal waters within 10 Å from the QM region were allowed to be minimized, while the rest of the system was kept frozen. The four models mentioned above were subjected to QM/MM minimization to optimize the geometry of the catalytic zinc environment. We employed the M06-2X functional[42] in combination with 6-31G(d,p)[43] basis sets to optimize the geometry of the catalytic zinc environment. Geometry optimizations were performed using an Amber12[44]–Gaussian09[45] QM/MM interface.[46] To compare with a previous study on ADH,[12,13] we present the optimization

DOI: 10.1021/cs501524k
ACS Catal. 2015, 5, 3207–3215

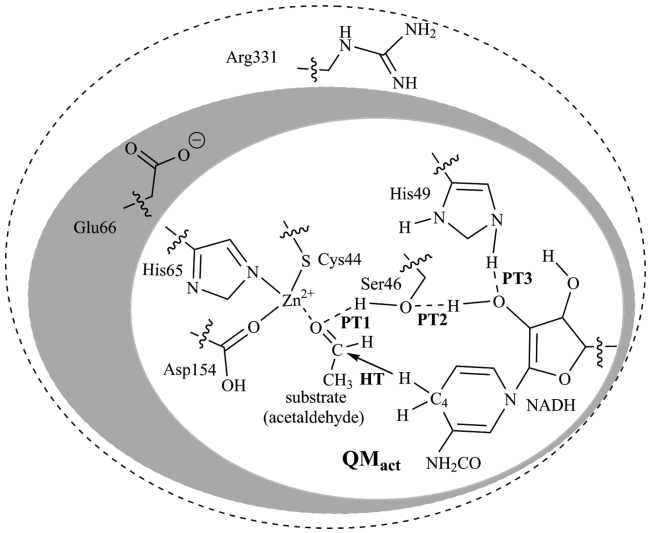

Figure 2. Three different QM models (QM_{act}, QM_{act}+Glu66 and QM_{act}+Glu66+Arg331) used to calculate the barriers for hydride transfer step in this study. Reduction reaction pathway including both hydride (HT) attack and proton transfer (PT) mechanism is shown.

results using the B3LYP functional in the Supporting Information (see Figure S1 and Table S1).

2.3. Steered QM/MM Molecular Dynamics Simulations. We employed the hybrid QM/MM scheme[47,48] to calculate the barriers for hydride transfer (HT) and proton transfer (PT) steps involved in the reduction of a carbonyl substrate by two alternative pathways, where QM part is treated using the PM6[49] semiempirical method and the MM part using the Amber99SB force field.[39] Semiempirical methods such as PM6 are suitable for large systems and allow free activation energy calculation, but the calculated barriers are overestimated by 10 kcal/mol or perhaps more.[50,51] The steered molecular dynamics simulation (SMD) approach implemented in Amber12 was used to force hydride transfer or proton transfer from either NADH cofactor or Ser46 to substrate, respectively. The simulations were carried out with the QM/MM PM6/ff99SB Hamiltonian using a linear combination of distances (LCOD)[37] for driving the reaction coordinate (RC). RC for the HT step is defined as the distance difference (D1 − D2) of the transferred hydrogen (H) toward C of the carbonyl substrate (D1) and H to the C4 carbon of NADH (D2). The H atom of NADH cofactor was moved step by step toward the carbonyl carbon (C) of the substrate by applying strong harmonic constraint to force the reaction. In the second pathway, RC for PT is defined as the distance difference (D1 − D2) between the proton donor (OH group) of Ser46 (D1) and the carbonyl oxygen of the substrate (D2). Initially, the solvent and the ions were minimized followed by the whole system, using 3000 steps of steepest descent and 2000 steps of conjugate gradient. The minimized system was heated gradually from 0 to 300 K in 50 ps (using Langevin dynamics for temperature control). Afterward, QM/MM MD equilibration at 300 K (25 ps) was carried out using PM6/ff99SB. To stay as close as possible to the catalytic state or resting state obtained from the CPCR2 X-ray structure, we applied catalytic distance constraints ($Zn-CO_{substrate}$, $Zn-NE2_{His65}$, $Zn-OD2_{Asp154}$, $Zn-SG_{Cys44}$, $Zn-OE1_{Glu66}$) during energy minimization, heating, and equilibration steps. The equilibrated system was then further subjected to QM/MM SMD simulation for 25 ps at 300 K with a time step of 0.5 fs to calculate the barriers involved in the reaction process. The hydride or proton was transferred with a time step of 0.5 fs for 25 ps with 50000 steps and 50 integration windows (1000 steps per window) along the reaction coordinate from +1.25 to −1.25. We performed all calculations in forward and backward directions to ensure the absence of hysteresis effects. Additionally, we performed simulations with time steps of 0.1 fs for 25 ps with 250000 steps and 250 integration windows (1000 steps per window) and 0.5 fs for 50 ps with 100000 steps and 100 integration windows (1000 steps per window) along the reaction coordinate. The results of these simulations are shown in Figures S11 and S20 in the Supporting Information. The applied force constant was 1000 kcal/mol $Å^{-2}$. SHAKE[52] was turned off for the QM region during all QM/MM simulations. To calculate the QM/MM electrostatic interactions, a cutoff of 8 Å was used.

To study the effect of the conserved residue Glu66 on the barriers involved in the hydride transfer step, we examined three different sets of QM regions. As the crystal structure was solved without substrate, acetaldehyde substrate was docked in the catalytic site of CPCR2. For molecular docking purposes, a bonded model of the catalytic zinc ion (where the charge on zinc ion is 1.01+) and AM1-BCC charges[53] for the substrate were used. HF-RESP charges for the catalytic zinc environment are given in Table S9 in the Supporting Information. Molecular docking was performed using AutoDock4.2[54] in Yasara structure version 13.9.8.[55] Initially, 81 atoms were included in the QM region (QM_{act}) and subjected to QM/MM SMD simulations. The QM region includes carbonyl substrate (acetaldehyde) and the reactive part of the nicotinamide cofactor (NADH) along with three zinc-coordinating residue side chains: i.e., Cys44, His65, and Asp154. Additionally, Ser46 and His49 (protonated) were included in the QM region because of their involvement in the proton relay mechanism. To analyze the effect of Glu66 on reaction barriers further, we enlarged the QM region and included Glu66 depicted in the model QM_{act}+Glu66, having a total of 88 atoms. Finally, we included both Glu66 and Arg331 in the QM region, and in total we have 101 atoms in the model QM_{act}+Glu66+Arg331. Defined QM models are depicted in Figure 2. The overall charges of the QM_{act}, QM_{act}+Glu66, and QM_{act}+Glu66+Arg331 models are +1, 0, and +1, respectively. The QM/MM SMD simulations for calculating the barriers involved in the hydride transfer step were repeated five times, and average values for the computed barriers in kcal/mol were calculated.

All three models were subsequently minimized to have a reliable starting reactant complex using the QM/MM scheme implemented in Amber12. Throughout the study, we have used a PM6[49] semiempirical Hamiltonian which has been described to be qualitatively consistent with the DFT calculations.[56] PM3 has been described to be reliable for studying the catalytic mechanism for HLADH in an active site model system.[57]

3. RESULTS AND DISCUSSION

The main aim of this study is to clarify the effect of two different conformers of Glu66 (Glu_{in} and Glu_{out}) and two different positions of zinc ion (Zn_{cat} and Zn_{rest}) on the barriers involved in the hydride transfer step during CPCR2-catalyzed reduction of a carbonyl substrate. First, we will analyze two Glu66 conformers (Glu_{in} and Glu_{out}) and two positions of zinc ion (Zn_{cat} and Zn_{rest}) with QM/MM geometry optimizations to provide insight into which individual states comprise the

DOI: 10.1021/cs501524k
ACS Catal. 2015, 5, 3207−3215

Table 1. Comparison of Distances between Zinc-Coordinating and Catalytically Important Residues Involved in the Active Site of CPCR2 in QM/MM Optimized Structures Calculated at the M06-2X/6-31G(d,p)//ff99SB Level of Theory[a]

	interatomic distance (Å)			
atom pairs	**Zn_{rest}–Glu_{in}**	Zn_{rest}–Glu_{out}	Zn_{cat}–Glu_{in}	**Zn_{cat}–Glu_{out}**
Zn–S (Cys44)	2.35 (2.34)	2.30 (2.34)	2.36 (2.35)	2.38 (2.35)
Zn–NE2 (His65)	2.01 (2.01)	2.00 (2.01)	1.96 (2.10)	1.96 (2.10)
Zn–OD2 (Asp154)	1.96 (2.07)	1.93 (2.07)	1.95 (1.80)	1.95 (1.80)
Zn–O (Wat)	3.6 2(4.26)	2.03 (4.26)	1.99 (2.03)	1.98 (2.03)
Wat–OH (Ser46)	3.64 (2.30)	2.59 (2.30)	2.90 (2.30)	3.45 (2.30)
Zn–OE (Glu66)	1.96 (1.97)	4.98 (4.37)	4.84 (3.99)	5.19 (6.09)
OE (Glu66)–H (Arg331)	1.83 (2.28)	1.89 (1.83)	1.85 (2.28)	1.82 (1.83)

[a]Values in parentheses are from the CPCR2 X-ray crystal structure (PDB ID: 4C4O). States shown in boldface type correspond to local minima.

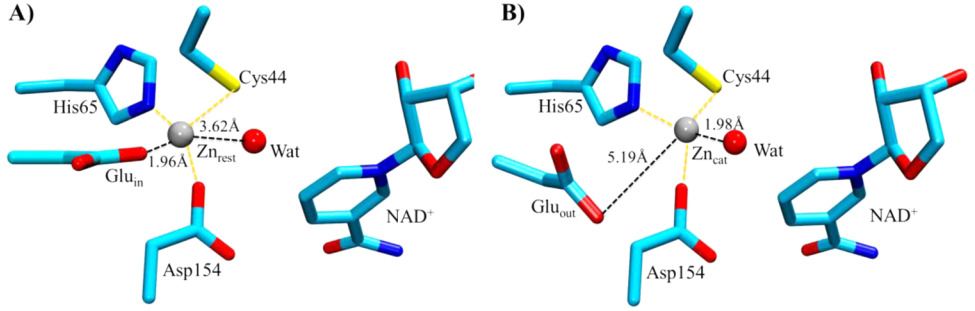

Figure 3. Catalytic zinc environments: (A) resting state (Zn_{rest}–Glu_{in}); (B) catalytic state (Zn_{cat}–Glu_{out}). Geometries were optimized at the QM/MM M06-2X/6-31G(d,p) level of theory. All of the coordinating residues (Cys44, His65, and Asp154) and crystal water as the fourth ligand along with NAD^+ cofactor are shown.

disorder seen in the X-ray structure. Then, we will present a detailed map of the reduction mechanism, including a hydride transfer step and proton relay pathway, using QM/MM SMD comparison of three different QM regions to investigate the importance of the strictly conserved Glu66 residue and its neighboring partner Arg331. In addition, we will describe a molecular dynamics simulation study of CPCR2 enzyme to investigate the movement of zinc ion from the catalytic state (Zn_{cat}) to the resting state (Zn_{rest}).

3.1. Geometry-Optimized Structures for Glu66 Conformers of CPCR2. In the subunit B of the X-ray crystal structure of CPCR2 (PDB ID: 4C4O),[10] two different side chain conformers of the residue Glu66 and two different positions for the catalytic zinc ion with occupancies of 50% are observed: namely, Zn_{rest} and Zn_{cat}, depicted in Figure 1. In one of the Glu66 (Glu_{in}) conformers the side chain is pointing toward the catalytic zinc ion, while in the other conformer (Glu_{out}) it is pointing away. The distances between two carboxylate oxygen atoms of Glu66 conformers toward Zn_{rest} are 1.96 and 4.98 Å, whereas with Zn_{cat} they are 4.84 and 5.19 Å, respectively (see Figure 1). The fourth coordination position of the zinc ion oriented toward the substrate binding site (Zn_{cat}) is occupied by crystal water, which is located at a distance of 2.03 Å, while for Zn_{rest} it is at a distance of 4.26 Å. The distances of the zinc-coordinating residues (Cys44, His65, and Asp154) to zinc ions in all cases remain in the ranges 2.30–2.38, 1.96–2.00, and 1.93–1.96 Å, respectively. The main aim behind the geometry optimization of a catalytic zinc environment is to identify the most predominant states of Glu66 conformers and possible associated positions of catalytic zinc ions, which can explain the disorder seen in the X-ray structure of CPCR2. The four possible models (Zn_{rest}–Glu_{in}, Zn_{rest}–Glu_{out}, Zn_{cat}–Glu_{in}, and Zn_{cat}–Glu_{out}) were minimized using QM/MM at the M06-2X/6-31G(d,p)//ff99SB level, and the resulting geometries (see Table 1) were compared. After geometry optimization of all four models, we primarily found only two minima for the Glu66 and zinc ion combination: namely, Zn_{rest}–Glu_{in} and Zn_{cat}–Glu_{out}.

In the minimized Zn_{rest}–Glu_{in} model, no remarkable geometry changes were observed; the Glu_{in} conformer remains intact on coordination to the Zn_{rest} ion with a distance of 1.96 Å, in comparison to 1.97 Å in the X-ray structure. This strong coordination of Zn_{rest} toward Glu66 does not allow the water molecule to act as a fourth ligand and to come close enough to the zinc ion (Zn_{rest}) and remains at a distance of 3.62 Å. However, in the Zn_{rest}–Glu_{out} model, Zn_{rest} moves to the position of Zn_{cat} and shows a direct coordination toward water after minimization with a distance of 2.03 Å vs 4.26 Å in the starting structure. Glu_{out} stays near its starting position after geometry optimization; thus, the observed minima correspond to the Zn_{cat}–Glu_{out} geometry.

Therefore, the Zn_{rest}–Glu_{out} model is not stable and converges barrierless into the Zn_{cat}–Glu_{out} state. Similar changes were also observed in the Zn_{cat}–Glu_{in} model, where zinc remains at its original position and Glu_{in} moves outward and occupies a position similar to that of Glu_{out} after geometry optimization, thus reaching again the Zn_{cat}–Glu_{out} geometry. Consequently, the Zn_{cat}–Glu_{out} model did not show any structural changes and remains near the starting coordinates from the X-ray structure during minimization. We conclude that the X-ray structure is not comprised of an independent overlay of four different geometries; a coupled state combination of either Zn_{cat} with Glu_{out} or Zn_{rest} with Glu_{in} seems to explain the disorder. Henceforth, we confirmed two minima after geometry optimization: i.e., the resting state (Zn_{rest}–Glu_{in}) and the catalytic state (Zn_{cat}–Glu_{out}), shown in Figure 3.

DOI: 10.1021/cs501524k
ACS Catal. 2015, 5, 3207–3215

3.2. Identification of the Fourth Ligand of Zn_{cat}. It has already been speculated that, in HLADH, a water molecule or a hydroxide ion (OH^-) may occupy the fourth coordination site of the zinc ion in the absence of substrate.[2] Using the catalytic state (Zn_{cat}–Glu_{out}) identified above as a model system, we inspected the hydrogen bond network and coordination distance of water toward Zn_{cat} and found that the distance for water is slightly longer (2.14 Å) than that in the crystal structure (2.03 Å) and the hydrogen bond between Ser46 and water is also elongated: 3.60 Å vs 2.30 Å. The Zn_{cat}–Glu_{out} distance (5.07 Å) after geometry optimization is lower by 1 Å than the crystal structure (6.09 Å) distance. Hence, we decided to introduce a hydroxide ion (OH^-) as a fourth zinc-coordinating ligand which could strengthen electrostatic interactions and the hydrogen bond network shown in Figure 4. The coordination distance of water toward Zn_{cat} is reduced to 1.93 Å, the H-bond distance toward Ser46 is 1.53 Å, and Glu66 is found 6.4 Å away. With this OH^- model, we were able to reproduce the interatomic distances for the catalytic state (Zn_{cat}–Glu_{out}) found in the crystal structure.

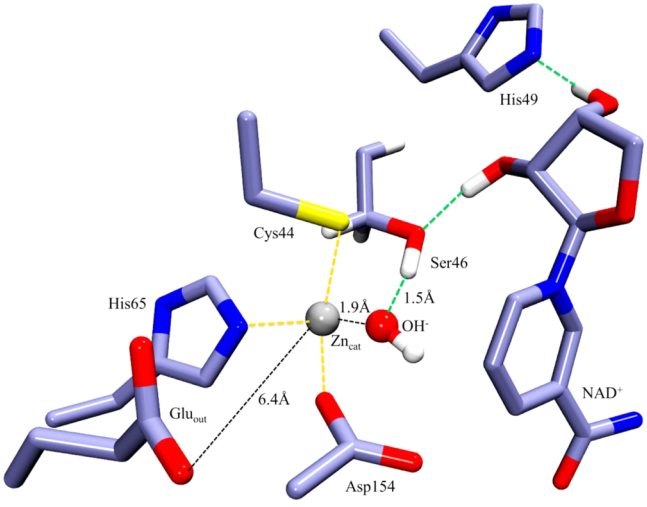

Figure 4. QM/MM M06-2X/6-31G(d,p) geometry optimized structure of the catalytic state (Zn_{cat}–Glu_{out}). All of the coordinating residues (Cys44, His65, and Asp154) and hydroxide ion as the fourth ligand along with the NAD^+ cofactor are shown; hydroxide ions (HO^-) are shown as ball and stick representations. The hydrogen bond network involving Ser46, the riboxyl group of NAD^+ cofactor, and His49 are shown.

3.3. Occurrence of Catalytic and Resting State PDB Structures of MDR. In the protein data bank (PDB), to date 136 structures of MDRs have been deposited. In most of them the catalytic zinc ion is coordinated to three amino acid ligands (Cys-His-Cys/Asp) and the fourth coordination site is occupied by a water molecule or substrate. In the holoenzyme of TbADH and its analog, ADH from *Clostridium beijerinckii* (CbADH),[58] the fourth coordination is occupied by conserved Glu60 residue, instead of a water molecule. This raises the question about the general importance of varying the tetrahedral coordination of the catalytic zinc ion. To study this more precisely, we analyzed the zinc-containing medium-chain dehydrogenases (MDR) within the PDB. Our analysis showed that only in 12% of available structures does the conserved glutamic acid residue coordinate to the catalytic zinc (resting state), while most commonly Glu stays away from the catalytic zinc (catalytic state). A detailed analysis is presented in Figure S12 in the Supporting Information. In the case of CPCR2, three monomers of the tetrameric enzyme are found in the resting state and one in a disordered state (vide infra). In three further structures of *Candida parapsilosis* carbonyl reductase (denoted CPR; PDB IDs 3WLE, 3WLF, and 3WNQ)[59] the enzyme is found in a catalytic state in the apo form with bound cofactor NAD^+, but in the resting state without cofactor, and consequently the bound ligand within the active center is not coordinated to the catalytic zinc ion. Additionally, we also analyzed the coupled movement of two different positions of Glu and catalytic zinc ion. We found that the crystal structure of human glutathione dependent formaldehyde dehydrogenase (PDB ID 2FZE)[28] contains two different positions of zinc (376) ion, Zn_{cat} 75% occupancy and Zn_{rest} 25%, in combination with a disordered Glu67, showing a high B factor. Glu67 is located at distances of 2.49 and 4.48 Å from the two resolved zinc ions, indicating an average disordered position between the Glu_{in} and Glu_{out} states. Therefore, the known crystal structure data can be explained using the previously discussed resting and catalytic states with coupled movement of zinc ion and conserved Glu behind the active site.

3.4. Reduction Reaction Mechanism of CPCR2 using QM/MM SMD Simulations. The plausible reduction mechanism of carbonyl reduction by CPCR2 consists of two steps; one is hydride transfer from NADH cofactor toward the carbonyl carbon of the substrate, and the other is a proton relay mechanism to protonate the alkoxide ion, schematically shown in Figure 2. In the hydride transfer step, the hydrogen from C4 of the nicotinamide moiety of the NADH cofactor is transferred to the carbonyl carbon of the substrate, while the carbonyl oxygen is activated via the catalytic zinc ion. The proton relay mechanism involves the neighboring Ser46, connected through a hydrogen bond network via the riboxyl group of NADH cofactor to the surface residue His49. To drive this reaction, we defined the reaction coordinate (see Computational Details) as transfer of the hydride from the cofactor to the substrate in our QM/MM SMD simulations.

3.4.1. Calculation of Reduction Reaction Path of CPCR2. In order to study the reaction path, we employed the Zn_{cat}–Glu_{out} model as the catalytic state with acetaldehyde coordinated as the fourth ligand to the zinc ion. The natural substrate of CPCR2 is not known; therefore, we have used acetaldehyde as a model carbonyl substrate to explore the reaction pathway. As the QM region we selected the QM_{act} model described in Figure 2. This model contains zinc-coordinating residues (Cys44, His65, and Asp154), Ser46, and His49 along with acetaldehyde and the nicotinamide moiety of NADH cofactor involved in the reduction reaction pathway. In the starting structure, the proposed catalytic hydrogen bond network involving the side chain of Ser46, pointing toward the carbonyl oxygen, the riboxyl group of the cofactor, and protonated His49 was present.

In Figure 5, the energy profile along the hydride transfer (defined by reaction coordinates) is shown. The free energy path of five independent QM/MM SMD runs shows an acetaldehyde reduction barrier of 36.9 kcal/mol with a standard deviation <1 kcal/mol closer to the midpoint of the hydride transfer pathway. The barrier for the reverse reaction is 21.1 kcal/mol for ethanol dehydrogenation. Since acetaldehyde is not the natural substrate for CPCR2, this explains the high barriers observed. In addition, we also calculated the barriers for better substrates taken from the recent study of CPCR2 in our

DOI: 10.1021/cs501524k
ACS Catal. 2015, 5, 3207–3215

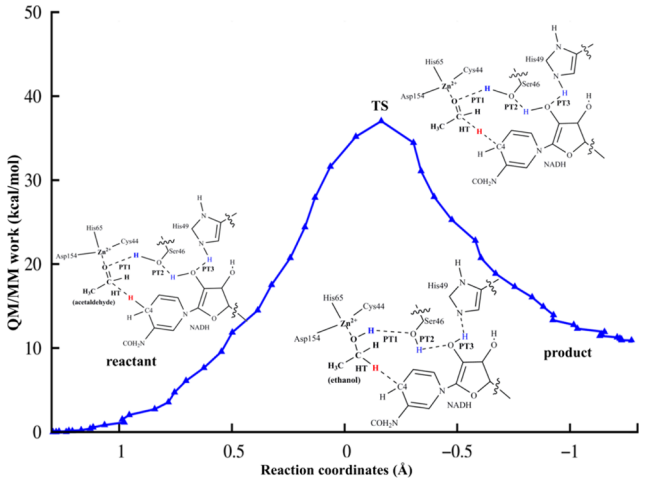

Figure 5. Energy profiles for the calculated barriers involved in the hydride transfer step using QM/MM SMD simulations along with the noticeable changes in the reaction coordinates during the reduction of carbonyl substrate: reactant, acetaldehyde; product, ethanol; TS, transition state region; hydride transfer, red; proton transfers, blue.

group.[8] The calculated reduction barrier for these substrates (methyl 3-oxopentanoate[8] and 2,3-hexanedione) using the QM_{act} model of the catalytic state (Zn_{cat}−Glu_{out}) was found to be lower than 30 kcal/mol and the dehydrogenation barriers are below 20 kcal/mol for 2,3-hexanedione, as shown in Table S10 in the Supporting Information. It is also known that semiempirical methods such as SCC-DFTB or PM3/6 overestimate the barrier for hydride transfer reactions in HLADH.[12,57,60] However, it is not expected that this changes the mechanistic conclusions for the resting and catalytic states drawn from our results. Benchmark calculations showed that high-level QM/MM calculations using MP2 and CCSD (coupled-cluster theory with single and double excitations) are needed to obtain more quantitative results for activation enthalpies.[50,51] The amount of tunneling in the hydride transfer reaction has been shown not to be dominant at 300 K for LbADH,[12,13] and the pathway does not deviate from the minimum energy path.

Inspection of the obtained transition state (TS) structures shows that the hydride is equidistant (1.4 Å) from both C atoms of the substrate and C4 of NADH cofactor. The angle C4−H−C is 160°, favoring a linear hydride transfer pathway. The distance between the carbonyl oxygen of substrate and zinc ion decreases from 2.6 Å in the starting structure to 2.0 Å, indicating carbonyl activation by the zinc ion. The geometrical parameters involved in the catalytic process throughout the SMD simulation are given in Tables S2−S7 in the Supporting Information. During the completion of hydride transfer, typically at reaction coordinate −0.25 Å (C−H distance <1.3 Å), the formed alkoxide ion was protonated spontaneously by the neighboring Ser46. Simultaneously, reprotonation of Ser46 via PT2 from riboxyl and reprotonation via PT3 from protonated His49 to riboxyl take place. This indicated that as soon as the hydride transfer takes place it is followed by barrierless simultaneous proton transfers, leading to the reduction of carbonyl substrate to the protonated alcohol. A typical trajectory of the catalytic reduction pathway is shown in a movie supplied as Supporting Information. The 3D-structures of the of active site of CPCR2 for the reactant, TS, and product taken from QM/MM SMD simulations for the QM_{act}+Glu66+Arg331 model of catalytic state (Zn_{cat}-Glu_{out}) are shown in Figure S8 in the Supporting Information. The calculations involving RC for HT step has been repeated with QM_{act} model in the backward direction using forward reaction coordinates as a starting point. The calculated barriers (QM/MM work) for both forward and backward direction shows no hysteresis effect and follow the same free energy path (see Figure S17 in the Supporting Information). Overlay of structures of the active site of CPCR2 for the forward, backward, and backward-forward reaction is shown in Figure S18 in the Supporting Information.

To explore the existence of an alternative pathway in the reduction of carbonyl substrate, we also calculated the barrier using SMD simulations driven by an initial proton transfer (PT1). In this SMD simulation, we pulled the proton from Ser46 to the carbonyl oxygen of substrate. As shown in Figure S10 in the Supporting Information, in these simulations the energy profile reaches a maximum of 40 kcal/mol after proton transfers. The protonated carbonyl (in contrast to the negatively charged alkoxide) detaches from zinc ion (distance >2.5 Å), and thus this pathway is not productive. Analysis of dynamics trajectories showed that all three proton transfer events (PT1, PT2, and PT3 in Figure 2) take place simultaneously, but no hydride transfer was observed (see Figure S9 in the Supporting Information). From these results, we conclude that the favorable pathway for the reduction of carbonyl substrates by ADHs involves a hydride transfer step followed by the sequential events of proton relay mechanism. This proposed pathway for reduction of carbonyl substrate via zinc-stabilized alkoxide formation follows the reverse of the order for the previously reported alcohol dehydrogenation pathway,[12,13] where the proton transfer is followed by a hydride abstraction. An alternative proton pathway in HLADH has been proposed by Luo and Bruice in 2001[61] and Esposito et al. in 2003,[30] in which the proton transfer takes place between the hydroxyl group of nicotinamide-ribose and the backbone carbonyl oxygen of Ile269. However, in the crystal structure of CPCR2, we found a large distance (>5 Å) between the riboxyl group of NADH cofactor (proton acceptor group) and the backbone carboxyl group of Phe237 (proton donor group). This ruled out the possibility of this alternative proton transfer pathway in CPCR2.

Additionally, we also calculated the barriers using a combination of RC for HT and PT events. The calculated barriers including only the RC for HT step (37.32 kcal/mol) was lower than that of a combination of RC for HT and PT events (RC for HT+1PT, HT+2PT, HT+3PT gives barriers of 41.79, 44.17, and 46.88 kcal/mol, respectively) shown in Figure S23 in the Supporting Information.

In order to investigate the minimum energy path, we have applied the QM/MM coupled nudged elastic band (NEB) method.[62−64] The reactant (acetaldehyde) and product (ethanol) structures were used as starting structures. Using NEB, we were able to locate the TS region (shown in Figure S25 in the Supporting Information) with the highest barrier for hydride transfer. The calculated barrier for HT using NEB was found to be 33.50 kcal/mol, close to the calculated barrier using QM/MM SMD simulations (36.9 kcal/mol). This identified TS region in NEB and SMD calculations is geometrically close to that of previously identified transition state structures[12,13] in which the hydride remains equidistant from the cofactor and the carbonyl carbon of substrate (see Table S11 in the Supporting Information). Our NEB calculations also suggested

DOI: 10.1021/cs501524k
ACS Catal. 2015, 5, 3207−3215

that the hydride transfer takes place first, followed by the proton transfer events (shown in Figure S24 in the Supporting Information) during carbonyl reduction.

3.4.2. Influence of Glu66 Position on the Barriers for the Reduction of Acetaldehyde. To investigate the role of the conserved Glu66 residue in the catalytic mechanism, we compared the barriers (Figure 6) for hydride transfer using

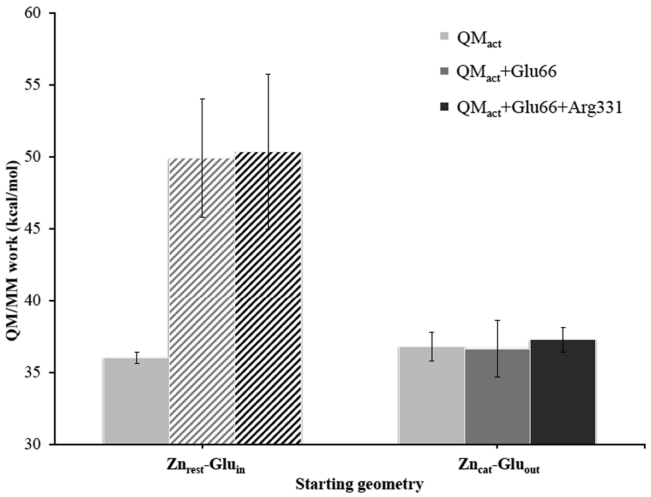

Figure 6. Calculated barriers for the hydride transfer step during the CPCR2-catalyzed reduction of a carbonyl substrate (acetaldehyde) using different QM region sizes, starting from the resting state (lined bars) and catalytic state (solid bars). The resting state with the QM$_{act}$ model relaxes to the catalytic state (Zn$_{cat}$−Glu$_{out}$) during SMD calculations. QM regions are shown in Figure 2. Error bars represent standard deviations.

two previously identified states, namely the resting (Zn$_{rest}$−Glu$_{in}$) and catalytic states (Zn$_{cat}$−Glu$_{out}$) as a starting structures. Our QM/MM SMD simulations using the QM$_{act}$ region of the resting state (Zn$_{rest}$−Glu$_{in}$) having Glu66 at a starting distance of 1.97 Å coordinated to zinc ion and 4.65 Å to the carbonyl substrate showed that the geometry converted to an arrangement similar to that of the catalytic state and a low barrier (36.0 kcal/mol) was obtained. Notably, Glu66 is not included in the QM region (QM$_{act}$), and therefore, we additionally included Glu66 and subsequently the adjacent Arg331 in the QM region. The resulting barriers for these QM regions are shown in Figure 6. In the second model using QM$_{act}$+Glu66 as the quantum region of our QM/MM SMD, Glu66 remains coordinated to the zinc ion (Zn$_{rest}$) throughout the reaction pathway calculations. The carbonyl group of the substrate is not coordinated to Zn$_{rest}$ (Zn−O distance >4.5 Å) in the reactant, TS, and product structures (see Figures S3 and S4 in the Supporting Information). Therefore, the resulting barriers are higher (49.9 kcal/mol) due to missing carbonyl activation by the zinc ion. Consistent average barriers (50.3 kcal/mol) were obtained when we treated Arg331 (QM$_{act}$+Glu66+Arg331) quantum mechanically. The barriers starting from the catalytic state are not influenced by including either Glu66 or Arg331 in the QM region.

To monitor the movement of catalytic zinc ion with respect to Glu66 and the coordinating residues (Cys44, His65, and Asp154), we defined a pseudo dihedral angle, as shown in Figure S15 in the Supporting Information. In the Zn$_{cat}$ position, the dihedral angle is +38°, which indicates it is above the plane of zinc-coordinating residues oriented toward the substrate binding pocket. In the Zn$_{rest}$ position, the dihedral angle is −41°, indicating orientation toward Glu66. We observed coupled movement of Zn$_{rest}$ to the Zn$_{cat}$ position and of Glu$_{in}$ to the Glu$_{out}$ position when Glu66 was treated by molecular mechanics (not allowing covalent coordination) in our QM/MM calculations. No mixed states, e.g. Zn$_{cat}$−Glu$_{in}$ and Zn$_{rest}$−Glu$_{out}$, were observed. We also performed classical molecular dynamics simulatiosn without substrate to investigate how the system would relax from either a catalytic or a resting state. In these simulations having NAD$^+$ and water in the binding site, the resting state remains stable and the catalytic state relaxes toward the resting state in 100 ps (see Figure S16 in the Supporting Information). As mentioned previously in zinc-dependent ADH from *Cupriavidus necator*,[26] the closed form can change to an open form (Glu66 coordinates to zinc ion), leading to release of product and exchange of cofactor, which increases the enzymatic turnovers. Similarly, our MD simulation results for CPCR2 also suggest that, in the absence of substrate, the catalytic state relaxes to the resting state and establishes the Glu66 coordination with the catalytic zinc ion. This relaxation to the resting state is important for product dissociation and cofactor exchange. This corresponds to the mutation studies of Glu residue,[22,23] which reduces the overall enzyme activity by impairing the dissociation of the product after chemical transformation.

4. CONCLUSIONS

In this paper, we have studied the reaction mechanism for reduction of a carbonyl substrate using CPCR2 by means of a QM/MM approach. With our QM/MM geometry optimizations, we obtained two minima (Zn$_{rest}$−Glu$_{in}$ and Zn$_{cat}$−Glu$_{out}$) of Glu66 conformers (Glu$_{in}$ and Glu$_{out}$) and zinc ion (Zn$_{cat}$ and Zn$_{rest}$). Our QM/MM SMD simulations show that the carbonyl reduction mechanism occurs through an initial hydride transfer step which donates H$^-$ to the carbonyl carbon followed by sequential events of barrierless proton transfer steps to protonate the generated alkoxide ion. Calculated barriers of the catalytic and resting states show that the catalytic state (Zn$_{cat}$−Glu$_{out}$) has a lower barrier for the hydride transfer step in comparison to the resting state (Zn$_{rest}$−Glu$_{in}$), indicating the influence of the Glu position on the reactivity of MDRs. This highlights the role of the coupled movement of conserved Glu and catalytic zinc in determining MDR structure and reactivity and sets the stage for a computational analysis of substrate specificity. More studies are in progress to identify the natural substrate for CPCR2, and high-level QM/MM calculations are needed to quantify the reaction barriers.

■ ASSOCIATED CONTENT

Supporting Information

The following files are available free of charge on the ACS Publications website at DOI: 10.1021/cs501524k.

Details of the QM/MM SMD simulation analysis, PDB analysis, and MD simulation results (PDF)

Movies of the catalytic state for QM/MM SMD simulations (MPG)

■ AUTHOR INFORMATION

Corresponding Author

*E-mail for M.B.: m.bocola@biotec.rwth-aachen.de.

Notes

The authors declare no competing financial interest.

DOI: 10.1021/cs501524k
ACS Catal. 2015, 5, 3207−3215

■ ACKNOWLEDGMENTS

G.V.D. and M.D.D. acknowledge DFG GRK 1166 BioNoCo for financial support. The authors thank Dr. Keyarash Sadeghian for carefully reading the manuscript.

■ ABBREVIATIONS

ADHs, alcohol dehydrogenases; SMD, steered molecular dynamics; QM/MM, quantum mechanics/molecular mechanics; MDR, medium-chain dehydrogenase/reductase; HLADH, horse liver alcohol dehydrogenase; FDH, formaldehyde dehydrogenase; PT, proton transfer; HT, hydride transfer; TbADH, *Thermoanaerobacter brockii* alcohol dehydrogenase; CbADH, *Clostridium beijerinckii* alcohol dehydrogenase

■ REFERENCES

(1) Eklund, H.; Samama, J.-P.; Wallén, L.; Brändén, C.-I.; Akeson, A.; Jones, T. A. *J. Mol. Biol.* **1981**, *146*, 561−587.
(2) Pettersson, G.; Klinman, J. P. *Crit. Rev. Biochem. Mol. Biol.* **1986**, *21*, 349−389.
(3) Eklund, H.; Branden, C. *Zinc enzymes*; Wiley: New York, 1983; pp 123−152
(4) Hedlund, J.; Jörnvall, H.; Persson, B. *BMC Bioinf.* **2010**, *11*, 534.
(5) Könst, P.; Merkens, H.; Kara, S.; Kochius, S.; Vogel, A.; Zuhse, R.; Holtmann, D.; Arends, I. W.; Hollmann, F. *Angew. Chem., Int. Ed.* **2012**, *51*, 9914−9917.
(6) Musa, M. M.; Phillips, R. S. *Catal. Sci. Technol.* **2011**, *1*, 1311−1323.
(7) Peters, J.; Minuth, T.; Kula, M.-R. *Enzyme Microb. Technol.* **1993**, *15*, 950−958.
(8) Jakoblinnert, A.; Bocola, M.; Bhattacharjee, M.; Steinsiek, S.; Bönitz-Dulat, M.; Schwaneberg, U.; Ansorge-Schumacher, M. B. *ChemBioChem* **2012**, *13*, 803−809.
(9) Jakoblinnert, A.; Wachtmeister, J.; Schukur, L.; Shivange, A. V.; Bocola, M.; Ansorge-Schumacher, M. B.; Schwaneberg, U. *Protein Eng., Des. Sel.* **2013**, *26*, 291−298.
(10) Man, H.; Loderer, C.; Ansorge-Schumacher, M. B.; Grogan, G. *ChemCatChem* **2014**, *6*, 1103−1111.
(11) Vallee, B. L.; Auld, D. S. *Biochemistry* **1990**, *29*, 5647−5659.
(12) Agarwal, P. K.; Webb, S. P.; Hammes-Schiffer, S. *J. Am. Chem. Soc.* **2000**, *122*, 4803−4812.
(13) Cui, Q.; Elstner, M.; Karplus, M. *J. Phys. Chem. B* **2002**, *106*, 2721−2740.
(14) Dudev, T.; Lim, C. *J. Am. Chem. Soc.* **2000**, *122*, 11146−11153.
(15) Dudev, T.; Cowan, J.; Lim, C. *J. Am. Chem. Soc.* **1999**, *121*, 7665−7673.
(16) Ryde, U. *Biophys. J.* **1999**, *77*, 2777−2787.
(17) Maynard, A.; Covell, D. *J. Am. Chem. Soc.* **2001**, *123*, 1047−1058.
(18) Lesburg, C. A.; Christianson, D. W. *J. Am. Chem. Soc.* **1995**, *117*, 6838−6844.
(19) Tiwari, M. K.; Singh, R. K.; Singh, R.; Jeya, M.; Zhao, H.; Lee, J.-K. *J. Biol. Chem.* **2012**, *287*, 19429−19439.
(20) Borras, T.; Persson, B.; Joernvall, H. *Biochemistry* **1989**, *28*, 6133−6139.
(21) Sun, H.-W.; Plapp, B. V. *J. Mol. Evol.* **1992**, *34*, 522−535.
(22) Ryde, U. *Protein Sci.* **1995**, *4*, 1124−1132.
(23) Ganzhorn, A.; Plapp, B. *J. Biol. Chem.* **1988**, *263*, 5446−5454.
(24) Kleifeld, O.; Shi, S. P.; Zarivach, R.; Eisenstein, M.; Sagi, I. *Protein Sci.* **2003**, *12*, 468−479.
(25) Sanghani, P. C.; Robinson, H.; Bosron, W. F.; Hurley, T. D. *Biochemistry* **2002**, *41*, 10778−10786.
(26) Kang, C.; Hayes, R.; Sanchez, E. J.; Webb, B. N.; Li, Q.; Hooper, T.; Nissen, M. S.; Xun, L. *Mol. Microbiol.* **2012**, *83*, 85−95.
(27) Eklund, H.; Ramaswamy, S. *Cell. Mol. Life Sci.* **2008**, *65*, 3907−3917.
(28) Sanghani, P. C.; Davis, W. I.; Zhai, L.; Robinson, H. *Biochemistry* **2006**, *45*, 4819−4830.
(29) Pauly, T. A.; Ekstrom, J. L.; Beebe, D. A.; Chrunyk, B.; Cunningham, D.; Griffor, M.; Kamath, A.; Lee, S. E.; Madura, R.; Mcguire, D. *Structure* **2003**, *11*, 1071−1085.
(30) Esposito, L.; Bruno, I.; Sica, F.; Raia, C. A.; Giordano, A.; Rossi, M.; Mazzarella, L.; Zagari, A. *Biochemistry* **2003**, *42*, 14397−14407.
(31) Senn, H. M.; Thiel, W. *Angew. Chem., Int. Ed.* **2009**, *48*, 1198−1229.
(32) Gordon, J. C.; Myers, J. B.; Folta, T.; Shoja, V.; Heath, L. S.; Onufriev, A. *Nucleic Acids Res.* **2005**, *33*, W368−W371.
(33) Wu, R.; Lu, Z.; Cao, Z.; Zhang, Y. *J. Chem. Theory Comput.* **2010**, *7*, 433−443.
(34) Wang, J.; Wolf, R. M.; Caldwell, J. W.; Kollman, P. A.; Case, D. A. *J. Comput. Chem.* **2004**, *25*, 1157−1174.
(35) Hellgren, M.; Carlsson, J.; Ostberg, L. J.; Staab, C. A.; Persson, B.; Hoog, J.-O. *Cell. Mol. Life Sci.* **2010**, *67*, 3005−3015.
(36) Pavelites, J. J.; Gao, J.; Bash, P. A.; Mackerell, A. D. *J. Comput. Chem.* **1997**, *18*, 221−239.
(37) Case, D.; Darden, T.; Cheatham, T.; Simmerling, C.; Wang, J.; Duke, R.; Luo, R.; Walker, R.; Zhang, W.; Merz, K. 2012, AMBER12 (San Francisco: University of California).
(38) Hornak, V.; Abel, R.; Okur, A.; Strockbine, B.; Roitberg, A.; Simmerling, C. *Proteins: Struct., Funct., Genet.* **2006**, *65*, 712−725.
(39) Cornell, W. D.; Cieplak, P.; Bayly, C. I.; Gould, I. R.; Merz, K. M.; Ferguson, D. M.; Spellmeyer, D. C.; Fox, T.; Caldwell, J. W.; Kollman, P. A. *J. Am. Chem. Soc.* **1995**, *117*, 5179−5197.
(40) Jorgensen, W. L.; Chandrasekhar, J.; Madura, J. D.; Impey, R. W.; Klein, M. L. *J. Chem. Phys.* **1983**, *79*, 926−935.
(41) Field, M. J.; Bash, P. A.; Karplus, M. *J. Comput. Chem.* **1990**, *11*, 700−733.
(42) Zhao, Y.; Truhlar, D. G. *Theor. Chem. Acc.* **2008**, *120*, 215−241.
(43) Pietro, W. J.; Hehre, W. J. *J. Comput. Chem.* **1983**, *4*, 241−251.
(44) Seabra, G. d. M.; Walker, R. C.; Elstner, M.; Case, D. A.; Roitberg, A. E. *J. Phys. Chem. A* **2007**, *111*, 5655−5664.
(45) Frisch, A. *Gaussian 09: User's Reference*; Gaussian, Inc.: Wallingford, CT, 2009.
(46) Götz, A. W.; Clark, M. A.; Walker, R. C. *J. Comput. Chem.* **2014**, *35*, 95−108.
(47) Burton, N.; Harrison, M.; Hart, J.; Hillier, I. *Faraday Discuss.* **1998**, *110*, 463−475.
(48) Nicoll, R. M.; Hindle, S. A.; MacKenzie, G.; Hillier, I. H.; Burton, N. A. *Theor. Chem. Acc.* **2001**, *106*, 105−112.
(49) Stewart, J. J. *J. Mol. Model.* **2007**, *13*, 1173−1213.
(50) Claeyssens, F.; Harvey, J. N.; Manby, F. R.; Mata, R. A.; Mulholland, A. J.; Ranaghan, K. E.; Schütz, M.; Thiel, S.; Thiel, W.; Werner, H. J. *Angew. Chem.* **2006**, *118*, 7010−7013.
(51) Korth, M.; Thiel, W. *J. Chem. Theory Comput.* **2011**, *7*, 2929−2936.
(52) Ryckaert, J.-P.; Ciccotti, G.; Berendsen, H. J. *J. Comput. Phys.* **1977**, *23*, 327−341.
(53) Jakalian, A.; Jack, D. B.; Bayly, C. I. *J. Comput. Chem.* **2002**, *23*, 1623−1641.
(54) Morris, G. M.; Huey, R.; Lindstrom, W.; Sanner, M. F.; Belew, R. K.; Goodsell, D. S.; Olson, A. J. *J. Comput. Chem.* **2009**, *30*, 2785−2791.
(55) Krieger, E.; Koraimann, G.; Vriend, G. *Proteins: Struct., Funct., Genet.* **2002**, *47*, 393−402.
(56) Schenker, S.; Schneider, C.; Tsogoeva, S. B.; Clark, T. *J. Chem. Theory Comput.* **2011**, *7*, 3586−3595.
(57) Olson, L. P.; Luo, J.; Almarsson, Ö.; Bruice, T. C. *Biochemistry* **1996**, *35*, 9782−9791.
(58) Korkhin, Y.; Peretz, M.; Bogin, O.; Burstein, Y.; Frolow, F. *J. Mol. Biol.* **1998**, *278*, 967−981.
(59) Wang, S.; Nie, Y.; Xu, Y.; Zhang, R.; Ko, T.-P.; Huang, C.-H.; Chan, H.-C.; Guo, R.-T.; Xiao, R. *Chem. Commun.* **2014**, *50*, 7770−7772.
(60) Alhambra, C.; Corchado, J. C.; Sanchez, M. L.; Gao, J.; Truhlar, D. G. *J. Am. Chem. Soc.* **2000**, *122*, 8197−8203.
(61) Luo, J.; Bruice, T. C. *J. Am. Chem. Soc.* **2001**, *123*, 11952−11959.

DOI: 10.1021/cs501524k
ACS Catal. 2015, 5, 3207−3215

(62) Mathews, D. H.; Case, D. A. *J. Mol. Biol.* **2006**, *357*, 1683−1693.
(63) Jönsson, H.; Mills, G.; Jacobsen, K. W. In *Classical and Quantum Dynamics in Condensed Phase Simulations*; Berne, B. J., Ciccoti, G., Coker, D. F., Eds.; World Scientific: Singapore, 1998; pp 385−404.
(64) Henkelman, G.; Jónsson, H. *J. Chem. Phys.* **2000**, *113*, 9978−9985.

DOI: 10.1021/cs501524k
ACS Catal. 2015, 5, 3207−3215